CHAPTER III
MOLECULAR SELF-ASSEMBLY OF DIAMINE-BASED BENZOXAZINES DEVELOPED BY CONCERTED HYDROGEN BOND AND ITS TUNABLE MORPHOLOGY

Abstract

Up to the present, molecular assemblies under the contribution of hydrogen bond in combination with weak interactions and their consequent morphologies have been variously reported; however, how the systematic variation of the structure can fine-tune the morphologies has not yet been answered. The present work finds the answer through highly symmetric molecules, i.e. diamine-based benzoxazine dimers. This type of molecule develops unique molecular assemblies with their networks formed by the hydrogen bond at the terminal, while, at the same time, the hydrogen bonded frameworks are further controlled by the hydrophobic segment at the center of the molecule. When this happens, slight differences in hydrophobic alkyl chain lengths (**C2**, **C4**, **C6** and **C8**) bring a significant change to the molecular assemblies, resulting in tunable morphologies, i.e. spheres, needles and dendrites. The superimposition between the crystal lattice obtained from X-ray single crystal analysis and the electron diffraction pattern obtained from the transmission electron microscope allows us to identify the molecular alignment from single molecules to self-assembly until morphologies developed. The present work, for the first time, shows the case of symmetric molecules that the hydrophobic building block controls in hydrogen bond patterns, leading to the variation of molecular assemblies with tunable morphologies.

Keywords: Self-assembly, Hydrogen bonding, Benzoxazine, Tunable morphology.

3.1 Introduction

The understanding of supramolecular architectures of self-assemblies is an essential prerequisite to develop nanoscale materials with specific properties.[1-4]The self-assemblies organized through the noncovalent interactions, so-called weak interactions, i.e. hydrogen bond[5], π-π stacking[6], and hydrophobic van der Waals are reported to be one of the key factors. Under those weak interactions, the self-assemblies develop the well-defined supramolecular structures and direct the nano- or microscopic morphologies[7] to be, for example, micelles[8], vesicles[9-11], tubes[12], rods[13], wires[14-16], helices[17, 18], *etc.*[19-21]

Up to the present, self-assemblies with specific morphologies under the role of hydrogen bonds have been variously reported. Great attention is now being paid to hydrogen bonds in cooperation with other weak interactions such as π-π stacking and hydrophobic van der Waals since these systems can mimic the natural supramolecular structures to show definite nanostructures.[22-25] For example, Sun *et al.* showed the self-assembly of perylene- and lysine-containing molecules that create various morphologies based on the nanostructures under hydrogen bonds with π-π stacking.[17] Moyer *et al.* demonstrated the self-assembly of peptide amphiphile in twisting morphology due to the combination of hydrogen bonds of the peptide segment and the hydrophobic-hydrophobic tail in the molecule.[26]

Thus, the question arises as to whether the hydrogen bond can be systematically controlled by changing cooperative weak interactions among the molecules in order to direct the organization of self-assemblies and fine-tune the morphologies or not. This study considers the symmetric molecules with two hydroxyl groups at each terminal and the alkyl chains in between. The systematic variation of the alkyl chains might lead to easily visualized changes in self-assembly patterns and the consequent tunable morphologies.

Based on the above mentioned approach, mono-phenol based benzoxazine, which can be obtained from mono-phenol, formaldehyde, and amines, is a good molecule to apply since its ring opening always leads to *N,N'*-bis(2-hydroxybenzyl) alkylamines, namely benzoxazine dimers.[27, 28] Previously, it was demonstrated that strong inter- and intramolecular hydrogen bonds (N-H···O-H) of the dimers develop

self-assemblies. By simply changing monoamine to diamines as shown in Scheme 1, a series of satisfied symmetrical molecules can be obtained with the phenol units for hydrogen bonds at both terminals and the variable alkyl chains in between for tuning the hydrophobicity.

3.2 Experimental Section

3.2.1 Materials

2,4-dimethylphenol, ethylenediamine, butamethylenediamine, hexamethylenediamine, octamethylenediamine, deuterated dimethylsulfoxide (DMSO-d_6) and deuterated chloroform ($CDCl_3$) were purchased from Sigma-Aldrich. Formaldehyde solution (37%), 1,4-dioxane, 2-propanol, diethylether and chloroform were obtained from Wako Pure Chemical Industries. Sodium hydroxide and sodium sulfate anhydrous were received from Fluka. All chemicals were used as received.

3.2.2 Synthesis of 6,6',6",6"'-(ethane-1,2-diylbis(azanetriyl))tetrakis (methylene)tetrakis(2,4-dimethylphenol) (C2)

1,2-bis(6,8-dimethyl-2H-benzo[e][1,3]oxazin-3(4H)-yl)ethane was simply prepared similar to our previous report. In brief, 2,4-dimethylphenol (1.22g, 10 mmol), paraformaldehyde (0.63 g, 21 mmol) and ethylenediamine (0.33 ml, 5 mmol) in chloroform (5 ml) were stirred in the opened-bath at 70°C until the white solid was obtained. Then followed by ring-opening reaction by adding 2,4-dimethylphenol (1.22 g, 10 mmol) in chloroform (5 ml) and allowed stirring at 120°C until the yellow viscous solution was obtained. The crude product was further purified in a mixed solvent of chloroform and methanol (1:1, v/v). The white crystals were dried to yield C2 for 82%.

^{1}H NMR (500 MHz, DMSO): δ 2.05 (12H, *s*), 2.11 (12H, *s*), 2.85 (4H, *t*), 3.62 (8H, *s*), 6.63 (4H, *s*), 6.76 (4H, *s*), 9.29 (4H, *br*). ESI-MS: *m/z* 596.8.

3.2.3 Synthesis of 6,6',6",6"'-(butane-1,4 diylbis(azanetriyl)) tetrakis (methylene) tetrakis(2,4-dimethylphenol) (C4)

The preparation of C4 was similar to C2, C4 was prepared from 2,4-dimethylphenol (1.22 g, 10 mmol), paraformaldehyde (0.63 g, 21 mmol) and butamethylenediamine (0.44 g, 5 mmol) in chloroform (5 ml), after the white solid was obtained, followed by ring-opening reaction by adding 2,4-dimethylphenol (1.22 g, 10 mmol) in chloroform (5 ml) and allowed stirring at 120°C until the yellow viscous solution was obtained. The crude product was further purified with the same procedure as C2 to obtain white crystals were dried to yield C4 for 87%.

^{1}H NMR (500 MHz, DMSO): δ 1.41 (4H, *m*), 2.09 (12H, *s*), 2.14 (12H, *s*), 2.32 (4H, *t*), 3.56 (8H, *s*), 6.70 (4H, *s*), 6.78 (4H, *s*), 9.47 (4H, *br*). ESI-MS: *m/z* 624.85.

3.2.4 Synthesis of 6,6',6",6"'-(hexane-1,6-diylbis(azanetriyl))tetrakis (methylene)tetrakis(2,4-dimethylphenol) (C6)

The preparation of C6 was similar to C2, C6 was prepared from 2,4-dimethylphenol (1.22 g, 10 mmol), paraformaldehyde (0.63 g, 21 mmol) and hexamethylenediamine (0.58 g, 5 mmol) in chloroform (5 ml), after the white solid was obtained, followed by ring-opening reaction by adding 2,4-dimethylphenol (1.22 g, 10 mmol) in chloroform (5 ml) and allowed stirring at 120°C until the yellow viscous solution was obtained. The crude product was further purified with the same procedure as C2 to obtain white crystals were dried to yield C6 for 92%.

^{1}H NMR (500 MHz, DMSO): δ 1.04 (4H, *m*) 1.43 (4H, *m*), 2.08 (12H, *s*), 2.13 (12H, *s*), 2.33 (4H, *t*), 3.57 (8H, *s*), 6.70 (4H, *s*), 6.77 (4H, *s*), 9.49 (4H, *br*). ESI-MS: *m/z* 652.9.

3.2.5 Synthesis of 6,6',6",6"'-(octane-1,8-diylbis(azanetriyl))tetrakis (methylene)tetrakis(2,4-dimethylphenol) (C8)

The preparation of C8 was similar to C2, C8 was prepared from 2,4-dimethylphenol 1.22 g, 10 mmol), paraformaldehyde (0.63 g, 21 mmol) and octamethylenediamine (0.72 g, 5 mmol) in chloroform (5 ml), after the white solid

was obtained, followed by ring-opening reaction by adding 2,4-dimethylphenol (1.22 g, 10 mmol) in chloroform (5 ml) and allowed stirring at 120°C until the yellow viscous solution was obtained. The crude product was further purified with the same procedure as C2 to obtain white crystals were dried to yield C8 for 90%.

^{1}H NMR (500 MHz, DMSO): δ 1.06 (8H, *m*) 1.46 (4H, *m*), 2.09 (12H, *s*), 2.14 (12H, *s*), 2.36 (4H, *t*), 3.59 (8H, *s*), 6.71 (4H, *s*), 6.78 (4H, *s*), 9.46 (4H, *br*). ESI-MS: *m/z* 680.9.

3.2.6 Instruments and Characterization

The infrared spectra were recorded with 32 scan at resolution 2 cm^{-1} on a Thermo Nicolet Nexus 670 in the frequency range of 4000–400 cm^{-1} equipped with deuterated triglycinesulfate (DTGS) detector. The temperature dependence FTIR spectra were collected using an in-house temperature controller attachment. ^{1}H NMR spectra were recorded on a Bruker Ultrashield Plus NMR spectrometer operating at Larmor frequencies of 500.13 MHz. For spin-lattice relaxation time (T_1) measurements, T_1 value was evaluated from inversion recovery (π–τ–$\pi/2$) measurements at controlled temperature. Mass spectroscopy was analyzed by a Bruker micrOTOF II electrospray ionization mass spectrometer (ESI-MS). The particle sizes of the molecular assembly were determined at 25°C by a Malvern Zetasizer Nano Series with a detection angle of 173°. Single crystal structure analysis was carried out by a Rigaku R-axis Varimax X-ray diffractometer with graphite monochromated Mo Kα radiation at 296 K. The structures were determined by the direct method (SIR92) and refined by full-matrix least-squares on F^2 with a RAPID AUTO program. All non-hydrogen atoms were refined with anisotropic displacement parameters as well as the fractional coordinates. The single crystals were obtained from recrystallization in DMSO. The compounds were dissolved in DMSO as defined concentration, a drop of which was dispersed on an amorphous carbon film supported by a Cu grid for transmission electron microscopy. A Hitachi H-7650 transmission electron microscope (TEM) operating at an accelerating voltage of 200 kV and equipped with a double tilt holder was used for imaging and electron diffraction.

3.3 Results and Discussion

A series of diaminotetraphenol derivatives, hereinafter, diamine-based benzoxazine dimers, with methylene segmental length $-(CH_2)_n-$ with n = 2, 4, 6, and 8 were synthesized as shown in Scheme 3.1.

Scheme 3.1 Designed and synthesized model compounds.

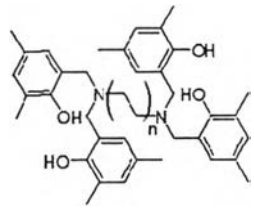

C2: n = 1
C4: n = 2
C6: n = 3
C8: n = 4

The molecular assemblies of **C2**, **C4**, **C6**, and **C8** via hydrogen bond in the solution state were examined by evaluating spin-lattice relaxation (T_1relaxation) using ^{1}H NMR in DMSO-d_6 under different concentrations and temperatures. T_1 relaxation is a parameter representing the energy exchange between individual nuclearspins and the surrounding liquid or solid lattice.[30, 31] Basically, when the molecules form an interaction with each other, the interaction obstructs the degree of freedom of the molecules resulting in the short T_1 relaxation time. Therefore, the differences in T_1 reflect the molecular self-assembly under the specific interaction, especially the hydrogen bond. To investigate this in detail, the hydroxyl protons at about 9.57 ppm were focused (Figure 3.1 (a)), and it was found that the T_1 value at this position significantly changes with the concentration. For example, in the case of **C2**, the value gradually decreased as the concentration increased, as it did for those of **C4** and **C6**, but more rapidly. This suggests that **C2**, **C4** and **C6** might be in a tight environment where hydroxyl group play the important role in forming intermolecular hydrogen network resulting in the self-assembly. It should be noted that hydrogen bond network of **C2** might be initiated in the different way with **C4** and **C6**, which shown in slightly decrease of T_1 value comparing to **C4** and **C6**. In the case of **C8**, the T_1 value did not show any significant change as the concentration increased. It

might be due to **C8** has no any intermolecular hydrogen bonding to create the self-assembly.

The size of self-assembly in solution was measured by dynamic light scattering (DLS) by using DMSO as solvent. Figure 3.1(b) shows that the size of **C2** is around 165 nm at the low concentration (1 mM) and gradually increases to 500 nm and to 1 μm when the concentrations reached 10 mM and 100 mM, respectively. Whereas **C4** and **C6** show the similar sizes of about 500 nm at the low concentration and become as large as 900 nm when the concentration is as high as 100 mM. In the case of **C8**, the particle size increases from 600 nm at 0.1 mM to 1 μm at 50 mM. Notably, when the concentration was up to 100 mM, the size rapidly increased to as high as 2.8 μm. This extremely increased in particle size of **C8** indicates that **C8** may not form the supramolecular assembly.

In fact, the T_1 values obtained from NMR and the particle sizes obtained from DLS, reflected the self-assembly phenomenon in solution state. This leads to the question that how the self-assembly forms in the solid-state. Thus, all derivatives were dissolved in DMSO with various concentrations before drying to observe the developed morphologies by TEM. In fact, chloroform and DMSO were good solvent to dissolve all compounds as high as 100 mM. However, in order to study the morphologies in the same condition as single crystal, DMSO was applied.

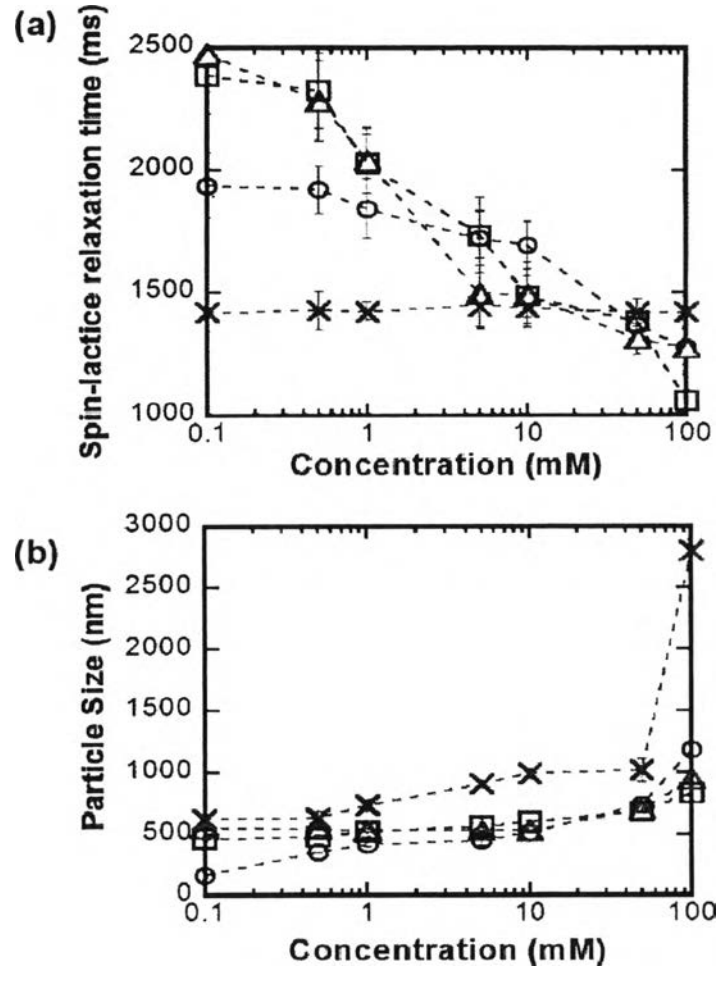

Figure 3.1 (a) Spin-lattice relaxation time (T_1) and (b) self-assembly particle size of **C2** (○), **C4** (Δ), **C6** (□), and **C8** (×) under varying concentrations.

As seen in Figure 3.2, the morphologies are found to be significantly fine-tuned by the concentrations. For example, **C2** changes from the donut-like at 0.001 mM to the round shape at 1.0 and 100 mM. Both **C4** and **C6** express the fiber morphology but with different branching. It is clear that **C8** shows irregular particles, especially in the low concentration (Figure 3.2 (j)).

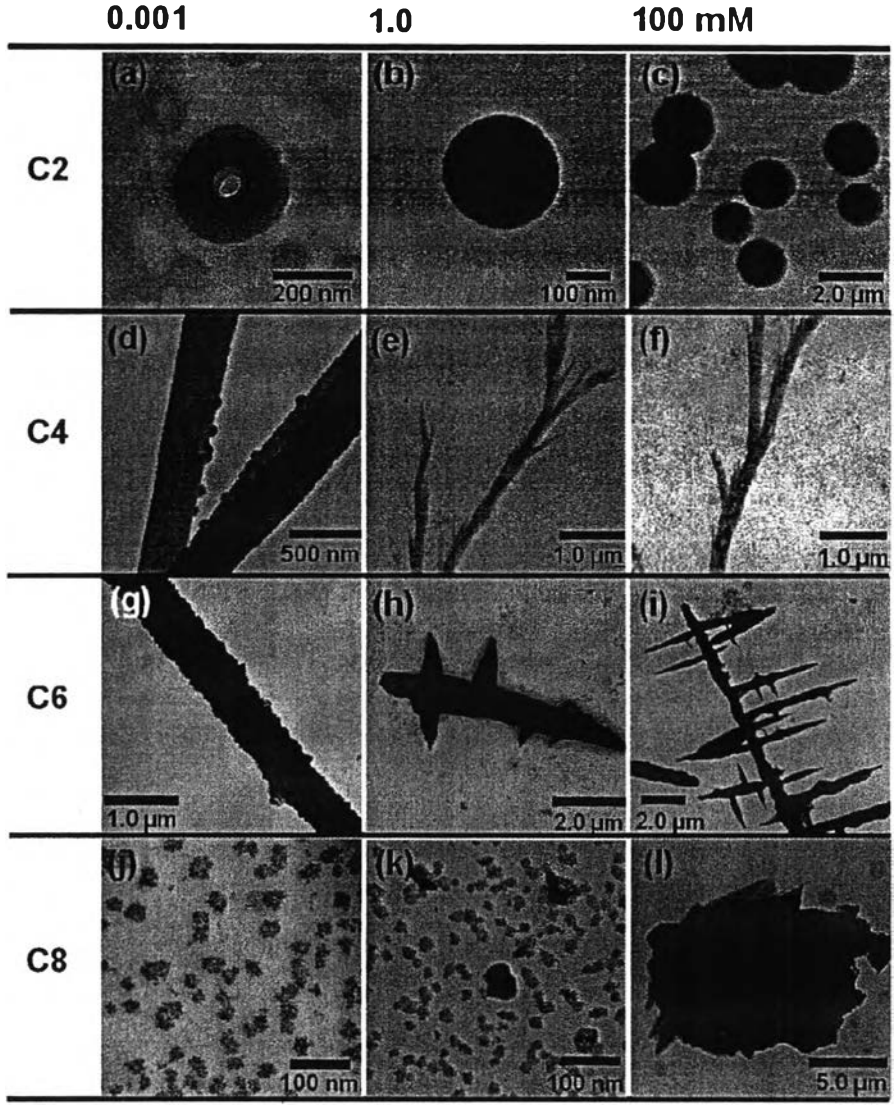

Figure 3.2 TEM micrographs of **C2**, **C4**, **C6**, and **C8** obtained from DMSO solutions with concentration of 0.001 mM for (a), (d), (g), and (f), concentration of 1.0 mM for (b), (e), (h), and (k), and concentration of 100 mM for (c), (f), (i), and (l).

For deeply investigation, the ^{1}H NMR spectra of **C2**, **C4**, **C6**, and **C8** recorded in DMSO-d_6 at room temperature contains signal of hydroxyl proton. At 50 °C, the signals of this proton remain broaden, indicating increased molecular motion because of destroyable aggregation.

As **C2**, **C4**, **C6**, and **C8** exhibit different morphologies; this implies how the alkyl chains - in other words, the methylene bridges - play a key role in the hydrogen bond formation. At this point, it could be pointed out that the molecular assembly formations were governed by the factors of the hydrogen bond pattern and alkyl bridge length, or hydrophobicity. To clarify this point, the crystal lattices were investigated using X-ray single crystal structure analyses. Here, the single crystals were grown slowly from the DMSO solutions, since chloroform didn't give the good crystals for us. As shown in Figure 3.3A (a), the **C2** crystal is in the triclinic system ($P\bar{1}$) with not only the intramolecular hydrogen bonds between N1 and O1 atoms, but also the intermolecular hydrogen bonds between O1 and O2 atoms with the distance of 2.84 Å. The molecules are in the extending, or stretching, structure. Figure 3.3B (a) illustrates the packing structures of **C2** by emphasizing the hydrogen bonds and tilting of the molecules. The **C4** is monoclinic ($P2_1/c$) with DMSO molecules entrapped in the unit cell (Figure 3.3A (b)). In this case, only the intramolecular hydrogen bond is observed, implying that the **C4** assembly is stabilized by the hydrogen bonds with the solvent molecules rather than by the intermolecular hydrogen bonds. The molecules are bridged together by the solvent molecules. For **C6**, the crystal structure is monoclinic ($C2/c$) with the intermolecular hydrogen bonds between O1 and O2 atoms along the c-axial direction (Figure 3.3A (c)). It is important to note that the crystal structure of **C6** in the connected molecular packing implies the possibility of a supramolecular polymer. For **C8**, the crystal structure is tetragonal ($P4_12_12$), where no intermolecular hydrogen bond exists in the crystal lattice. Only the intramolecular hydrogen bond is detected between N1 and O2 with the distance of 2.68Å and between O1 and O2 atoms with 2.83 Å distance (Figure 3.3A (d)). In other words, the molecules are in dimer-rings. From this analysis, it is clear that the systematic variation of the alkyl chain length affects the differences of hydrogen bond patterns and the packing mode for the unique morphologies formation.

Furthermore, in order to clarify the development of the molecular arrangement and hydrogen bond patterns in the assembly, the electron diffraction patterns obtained from the TEM measurements were compared with the X-ray diffraction patterns.

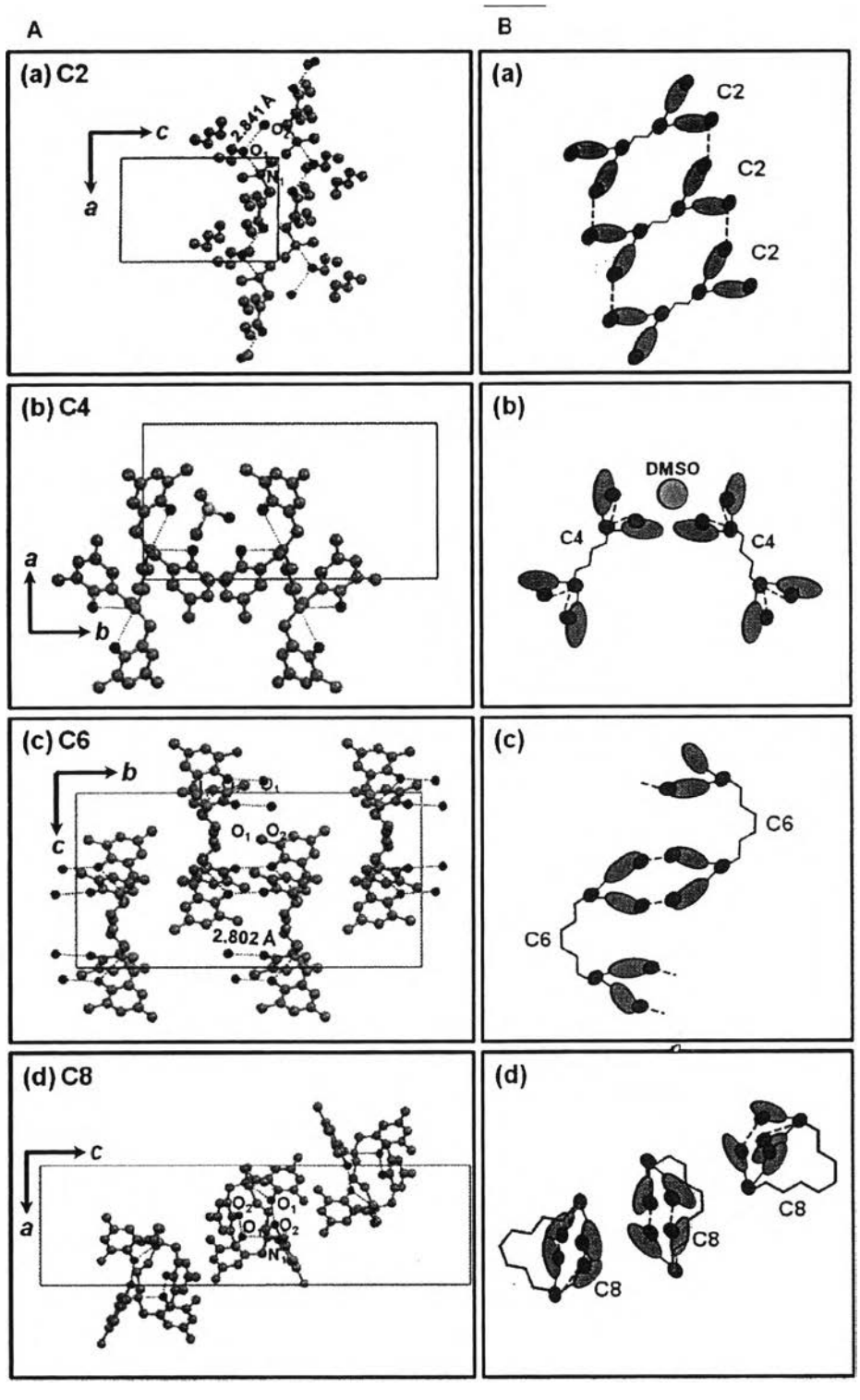

Figure 3.3 (A) Crystal structures and (B) schematic illustrations of the intra- and intermolecular hydrogen bonds and their types of packing structures: (a) **C2**, (the

extended packing), (b) **C4** (the solvent bridged packing), (c) **C6** (the connected molecular packing), and (d) **C8** (the dimer ring packing).

The TEM micrograph of **C2** shows the spherical morphology (Figure 3.4 (a)) with an average diameter of 250-500 nm (Figure 3.4 (b)). In the case of **C4**, the morphology shows the bunch of fibers with branches (Figure 3.4 (d)). The electron diffraction pattern shows the crystalline unit cells in the oriented fibers (Figure 3.4 (d)). The fibers are as long as tens of micrometers with the diameter ~200 nm. The morphology of **C8** is quite different from those of the others as it shows a random particulate shape. It is important to note that no clear spots were detected in the electron diffraction patterns for **C2** (Figure 3.4 (c)) and **C8**, implying that the molecular assemblies of both cases might not be in a highly ordered structure. Considering other results, especially from the X-ray single crystal analysis (Figures 3.2 (j), (k), (l) and Figure 3.3(d)), it is clear that the packing structure might be satisfied with only intramolecular hydrogen bonds until no molecular assembly can be formed.

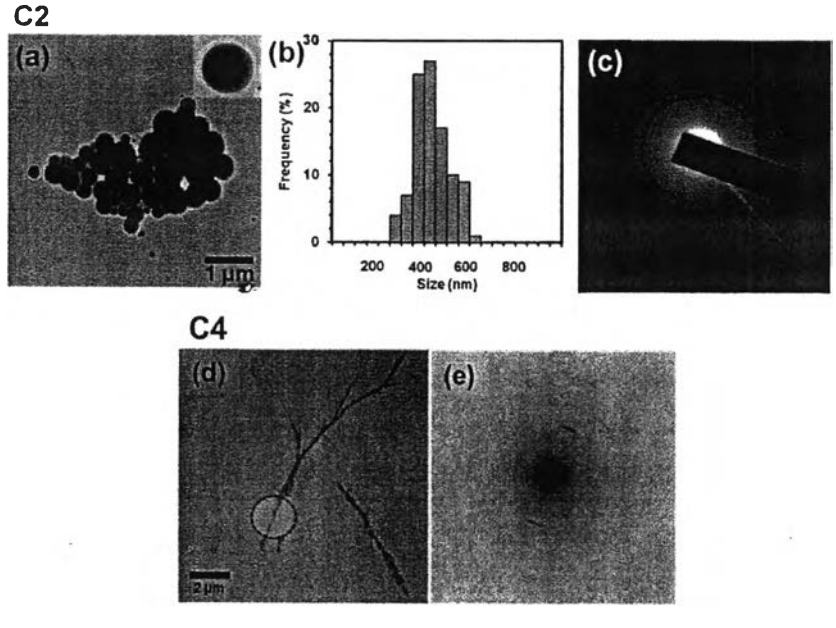

Figure 3.4 TEM micrographs of **C2**: (a) morphology, (b) size distribution, and (c) electron diffraction pattern, and of **C4**: (d) morphology, and (e) electron diffraction pattern.

As **C6** shows the dendritic needles (Figure 3.5 (a)), with a clear electron diffraction pattern (Figure 3.5 (b)), the detailed analysis was carried out. It should be pointed out that the diffraction pattern is relevant to the crystal structure identified by X-ray single crystal analysis; therefore, it is expected that the superimposition between two images (figure 3.5 (a) and (b)) might allow identification of the axis direction and growth of molecular assemblies. On the basis of the crystal structure information obtained from the X-ray structure analysis (Figure 3.3(c)), the electron diffraction pattern of **C6** with the orientation of crystallographic axes can be determined (Figure 3.5 (b)). The growing direction of the long needle is found to be parallel to the *a*-axis. The branches are stretching from the main needle in the [206] direction to grow along the *a*-axial direction individually (Figure 3.5 (a)).

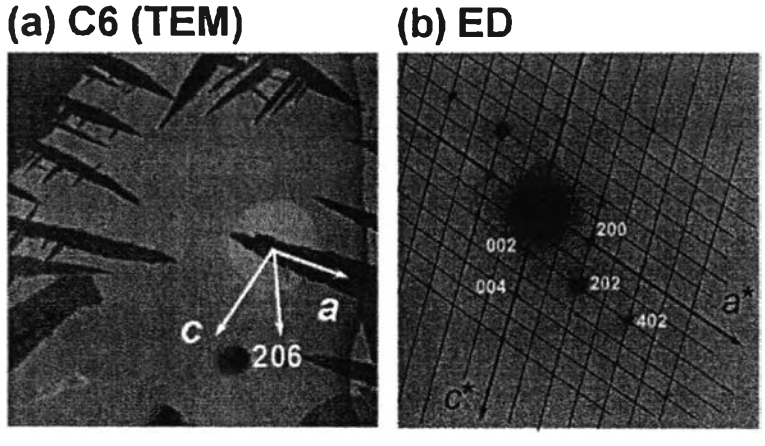

Figure 3.5 (a) TEM micrograph of **C6** with the crystal axes. The side branches are created along the [206] direction of the main needle, and (b) electron diffraction (ED) diagram taken from the main needle (the bright circle shown in (a)) and the indexing.

Although several cases of supramolecular structures and their unique morphologies were reported, the molecular alignment from single molecules to self-assembly until the definite morphologies developed is still the point to be clarified. Here, an attempt to illustrate the morphologies from the molecular level was carried out. Figure 3.6 is the scheme showing the growth of the needle crystallites of **C6** along the *a*-axial direction. At that time, the **C6** molecules are stacked in the *bc* plane

using intermolecular hydrogen bonds, and these stacked layers are attached onto the end of the needle crystallite in the growing process. It is expected that a similar situation might occur in the case of **C4** crystals.

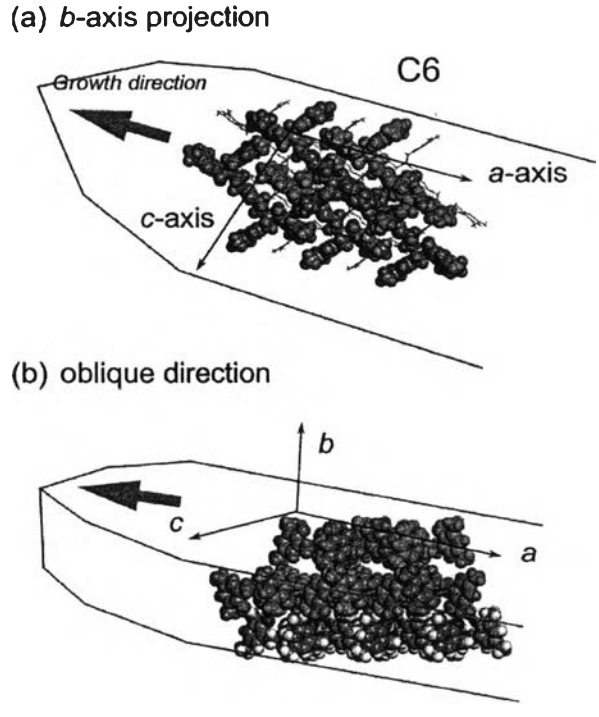

Figure 3.6 Schematic representation of needle growth of **C6** based on the superimposition of the needle axis and crystallographic axis: (a) *b*-axis projection and (b) the view from the oblique direction. The stacked molecular layers are attached step by step on the surface of the *bc* plane or along the *a*-axis.

Taking the effect of concentration as shown in Figure 3.2 back to our consideration, it is speculated that **C2-C6** might form the nanostructures based on the hydrogen bond networks which were under the effect of alkyl chains. In other words, the hydrophobic alkyl chains played an important role to control the packing structure on top of the intermolecular hydrogen bonds. Therefore, when the concentration increased, the packing structure might be developed differently as a consequence of hydrophobic interaction. In this way, for example **C2** either in the

low concentration or in the high concentration, it shares the common mechanism as mentioned above, the sphere at high concentration might be a consequence of tightly packed assemblies under the two methylene unit of alkyl chain. The common mechanism, but depending on the alkyl chain length, can also be seen in the cases of **C4**, and **C6** (Figure 3.2) which the branching and dendritic were developed at the high concentration.

It is known that self-assembly and its definite morphology can be tuned depending on the environments such as concentration[22, 32], temperature[33], pH[34], drying methods[12], and types of solvent.[35] As chloroform is also a good solvent of these derivatives, their morphologies were observed to see how the environment affects molecular assemblies. Figure 3.7 shows the morphologies of all derivatives obtained by 1.0 mM concentration. It is clear that **C2** performs its spherical shape, whereas **C4** and **C6** show the fine needle shape. The results are similar to those obtained from DMSO.

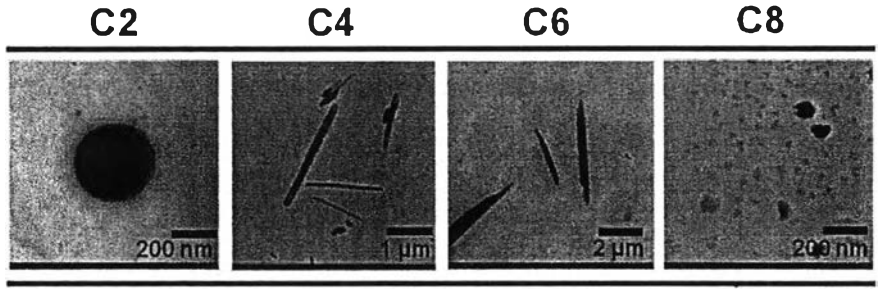

Figure 3.7 TEM micrographs of **C2**, **C4**, **C6**, and **C8** molecular assemblies obtained from the $CHCl_3$ solutions at the concentration of 1.0 mM.

3.4 Conclusions

Diamine-based benzoxazine dimers represents a good example of the molecular assembly that can be fine-tuned by simply varying the alkyl building blocks of the molecules. The single crystal structure analysis as well as the superimposition between X-ray single crystal structure and electron diffraction pattern insisted that the molecular assemblies were basically formed by the hydrogen

bonds, while they were further governed by the hydrophobic segment to tilt the packing structures. Therefore, the variation of the alkyl chain units and the concentration brought a significant change of the nano-scale structures to be donuts, spheres, needles, and dendrites. In addition, the solvent, such as DMSO, might also contribute to the supramolecular network. The present work, for the first time, shows the molecular assemblies under the hydrogen bond networks which were, in fact, primarily controlled by the hydrophobicity of the molecules.

3.5 Acknowledgement

The work was supported by the 90th Anniversay of Chulalongkorn University Fund (Ratchadaphiseksomphot Endowment Fund) and Basic Research Grant (BRG5380010). One of the authors, P. T., would like to acknowledge the scholarships from Royal Golden Jubilee, Thailand Research Fund (PHD/0067/2553, 2L.CU/53/F.2) and Japan Student Services Organization (JASSO). The authors would like to extend their gratitude to Professor Kohji Tashiro, Toyota Technological Institute, for his supports and good collaboration, Dr. Taiyo Yoshioka for TEM-electron diffraction measurement. The authors acknowledge Hitachi High Technology, Japan for TEM measurement.

3.6 References

1. A. Barnard, P. Posocco, S. Pricl, M. Calderon, R. Haag, M. E. Hwang, V. W. T. Shum, D. W. Pack and D. K. Smith, Journal of the American Chemical Society, **2011**, 133, 20288-20300.
2. P. Rajamalli and E. Prasad, Langmuir, **2013**, 29, 1609-1617.
3. K. Ariga, T. Nakanishi and J. P. Hill, Current Opinion in Colloid & Interface Science, **2007**, 12, 106-120.
4. Y. B. Zheng, B. K. Pathem, J. N. Hohman, J. C. Thomas, M. Kim and P. S. Weiss, Advanced Materials, **2013**, 25, 302-312.

5. Y. Yang, W. Feng, J. Hu, S. Zou, R. Gao, K. Yamato, M. Kline, Z. Cai, Y. Gao, Y. Wang, Y. Li, Y. Yang, L. Yuan, X. C. Zeng and B. Gong, Journal of the American Chemical Society, **2011**, 133, 18590-18593.
6. S. Lee, S. Oh, J. Lee, Y. Malpani, Y.-S. Jung, B. Kang, J. Y. Lee, K. Ozasa, T. Isoshima, S. Y. Lee, M. Hara, D. Hashizume and J.-M. Kim, Langmuir, **2013**, 29, 5869-5877.
7. P. Bombicz, T. Gruber, C. Fischer, E. Weber and A. Kalman, CrystEngComm, **2014**, 16, 3646-3654.
8. J. He, X. Huang, Y.-C. Li, Y. Liu, T. Babu, M. A. Aronova, S. Wang, Z. Lu, X. Chen and Z. Nie, Journal of the American Chemical Society, **2013**, 135, 7974-7984.
9. M. Antonietti and S. Förster, Advanced Materials, **2003**, 15, 1323-1333.
10. S. Chiruvolu, S. Walker, J. Israelachvili, F. J. Schmitt, D. Leckband and J. A. Zasadzinski, Science (New York, N.Y.), **1994**, 264, 1753-1756.
11. T. Sun, Q. Guo, C. Zhang, J. Hao, P. Xing, J. Su, S. Li, A. Hao and G. Liu, Langmuir, **2012**, 28, 8625-8636.
12. G. Sun and C.-C. Chu, ACS Nano, **2009**, 3, 1176-1182.
13. A. Aggeli, I. A. Nyrkova, M. Bell, R. Harding, L. Carrick, T. C. B. McLeish, A. N. Semenov and N. Boden, Proceedings of the National Academy of Sciences of the United States of America, **2001**, 98, 11857-11862.
14. C. Li, M. Numata, A.-H. Bae, K. Sakurai and S. Shinkai, Journal of the American Chemical Society, **2005**, 127, 4548-4549.
15. J. Puigmarti-Luis, A. Minoia, S. Lei, V. Geskin, B. Li, R. Lazzaroni, S. De Feyter and D. B. Amabilino, Chemical Science, **2011**, 2, 1945-1951.
16. S. V. Rosokha, C. L. Stern and J. T. Ritzert, CrystEngComm, **2013**, 15, 10638-10647.
17. Y. Sun, C. He, K. Sun, Y. Li, H. Dong, Z. Wang and Z. Li, Langmuir, **2011**, 27, 11364-11371.
18. S. Ahmed, J. H. Mondal, N. Behera and D. Das, Langmuir, **2013**, 29, 14274-14283.

19. S.-C. Lin, T.-F. Lin, R.-M. Ho, C.-Y. Chang and C.-S. Hsu, Advanced Functional Materials, **2008**, 18, 3386-3394.

20. B. Donnio, S. Buathong, I. Bury and D. Guillon, Chemical Society Reviews, **2007**, 36, 1495-1513.

21. A. Vidyasagar, K. Handore and K. M. Sureshan, Angewandte Chemie International Edition, **2011**, 50, 8021-8024.

22. L. C. Palmer and S. I. Stupp, Accounts of Chemical Research, **2008**, 41, 1674-1684.

23. X. Zhang and C. Wang, Chemical Society Reviews, **2011**, 40, 94-101.

24. L. Xu, X. Miao, B. Zha, K. Miao and W. Deng, J. Phys. Chem. C, **2013**, 117, 12707-12714.

25. D. S. Janni and M. K. Manheri, Langmuir, **2013**, 29, 15182-15190.

26. T. J. Moyer, H. Cui and S. I. Stupp, J. Phys. Chem. B, **2012**, 117, 4604-4610.

27. A. Laobuthee, S. Chirachanchai, H. Ishida and K. Tashiro, J. Am. Chem. Soc., **2001**, 123, 9947-9955.

28. S. Phongtamrug, K. Tashiro, M. Miyata and S. Chirachanchai, J. Phys. Chem. B, **2006**, 110, 21365-21370.

29. C. S. Higham, D. P. Dowling, J. L. Shaw, A. Cetin, C. J. Ziegler and J. R. Farrell, Tetrahedron Letters, **2006**, 47, 4419-4423.

30. L. Yuan, H. Zeng, K. Yamato, A. R. Sanford, W. Feng, H. S. Atreya, D. K. Sukumaran, T. Szyperski and B. Gong, Journal of the American Chemical Society, **2004**, 126, 16528-16537.

31. L. Brunsveld, H. Zhang, M. Glasbeek, J. A. J. M. Vekemans and E. W. Meijer, Journal of the American Chemical Society, **2000**, 122, 6175-6182.

32. M. M. J. Smulders, M. M. L. Nieuwenhuizen, M. Grossman, I. A. W. Filot, C. C. Lee, T. F. A. de Greef, A. P. H. J. Schenning, A. R. A. Palmans and E. W. Meijer, Macromolecules, **2011**, 44, 6581-6587.

33. C. Marie, F. Silly, L. Tortech, K. Müllen and D. Fichou, ACS Nano, **2010**, 4, 1288-1292.

34. M. T. Fenske, W. Meyer-Zaika, H.-G. Korth, H. Vieker, A. Turchanin and C. Schmuck, Journal of the American Chemical Society, **2013**, 135, 8342-8349.

35. A. K. Boal, F. Ilhan, J. E. DeRouchey, T. Thurn-Albrecht, T. P. Russell and V. M. Rotello, Nature, **2000**, 404, 746-748.